Journal of Microelectronics and Electronic Packaging (2010) **7**, 205-213
Copyright © International Microelectronics And Packaging Society
ISSN: 1551-4897

Inkjet Printing of Fine-Line Thick-Film Inductors

Marcel Wassmer, Waldemar Diel, and Klaus Krueger

***Abstract*—Inkjet printing is the emerging technology for the deposition of a variety of particles. The reliable printing of nano-silver inks shows the possibilities of digital fabrication of microelectronic circuits and raises the question for further use with other particles. To compete with common thick-film screen printing as a production method it is consequential and necessary to investigate the inkjet printing of all passive electronic thick-film components. Inductors are frequently required in electronic circuits, yet they represent a main challenge for thick-film printing. With the development of new materials, which are suitable for low-temperature cofired ceramic processes, the integration of passive components promises new applications.**

In a first step, different ferrite particle compositions are dispersed to stabilized inks that can be used with a commercial inkjet print head. The stability of the ink is fundamental for reliable drop formation. In addition, the viscosity must fit to the print heads' operational ranges and the magnetic properties must be taken into account. In a second step, the effect of substrate coating and drop volume variation toward the shape of the printed structures are defined and shown. The fundamental construction methods of inkjet-printed inductors on fired ceramic are investigated. First, silver coils are printed without ferrite to optimize the printing pattern. Subsequently, coils are embedded in inkjet printed ferrite layers.

Depending on the geometrical layout, several drying and firing steps are necessary, leading to a more complex production process and influencing the electrical properties. Finally, it is shown that inkjet printing is very effective for built-up of multilayer thick-film inductors, and the high accuracy of the printing process promises accurate electrical values.

***Keywords*—Inkjet, inductor, thick-film, contact angle, ferrite**

Introduction

Inkjet printing is a flexible and material-saving technology for digital fabrication of thick-film microelectronic circuits. The basis of electronic circuits are conductive silver lines that might consist of nano-silver particles [1, 2]. As the most important influences on ink composition and stability are well known [3], inkjet printing becomes more reliable and thus applicable for thick-film printing. Another step of investigation necessarily should be the realization of other passive components by ink-jet printing. New high-k particle compositions for thick-film screen printing promise high capacitances and compatibility with low-temperature cofired ceramic (LTCC) substrates [4, 5]. This is achieved by inorganic additives and particle size reduction [6]. Whereas smaller particles are a challenge for conventional screen printing, they simplify inkjet printing. These particles allow inkjet printing of thick-film capacitors of variable capacitances [7]. New ferrite particle compositions [8] for LTCC tape production with high relative permittivity also promise the integration of inductive components as embedded elements with an elevated inductance [9, 10]. Compared with the integration of a complete ferrite tape into LTCC stack, inkjet printing of ferrite layers is more flexible toward circuit design, and later it promises material saving.

Considering the printing process, the particles have to be suitably dispersed and stabilized. The solvents and the dispersants need to fit to particle composition and print head requirements [11, 12]. However, the interaction between ink and substrate, especially the resulting contact angle, must also be taken into account to achieve fine and reliable structures as required for inductor coils.

Considering the existing knowledge of inkjet-printed conductor lines and capacitors [2, 7], it is consequential to investigate the realization of inductors. Although the fundamental construction rules do not differ from screen printing, the behavior of the inks differs significantly from that of pastes. Thus, an adaptation of the whole process is required.

Methods

For the first experiments, a few pastes are prepared and ink formulations are tested for compatibility, stability, viscosity, and reliability. After identifying compatible and stable ink compositions, the inks are printed with the commercial Xenjet4000 printer on fired alumina substrates to evaluate the drop parameters as well as the drying and flow behavior. The corresponding print head, Xaar HSS 1001, has 1000 active nozzles of 25 μm diameter. The substrate is fixed by vacuum and intermediately heated, alternatively by an infrared lamp, or hot air, to a temperature of approximately 80°C. In addition, substrates with two different coatings are investigated to analyze drying behavior. For each ink, a printing test is run with different patterns, i.e., the line-width to space-width ratio is varied to find the best possible printing conditions.

With different line/space pitches and different layer thicknesses, meander shaped as well as square flat spiral inductors are built up using inkjet printing. Later, similar conductors are printed again between ferrite layers. Finally, the geometrical and electrical properties of the elements are investigated.

Ink Preparation

The preparation of a suitable ink is based on two essential steps. Initially, a paste with high solid substance content is

Manuscript received July 2010 and accepted January 2011
Institute of Automation Technology, Helmut-Schmidt-University/University of the German Armed Forces, 22043 Hamburg, Germany
*Corresponding author; email: klaus.krueger@hsu-hh.de

doi:10.4071/imaps.258 1551-4897 © 2010 International Microelectronics And Packaging Society

Downloaded from http://meridian.allenpress.com/jmep/article-pdf/7/4/205/2258973/imaps_258.pdf by guest on 01 November 2022

Table I
Properties of the Used Particles

	Ferrite	Ag
d_{90} in µm	0.15	0.46
d_{50} in µm	0.1	0.30
Surface Area in m^2/g	35.10	2.71
Bulk Density in g/cm^3	5.36	10.49

Table II
Used Solvents

	Description
Sol. 1	2-(2-Butoxyethoxy)-ethanol
Sol. 2	[2-2(-Butoxyethoxy)-ethyl]-acetat
Sol. 3	2-Butoxyethanol

prepared. Afterward, the paste is diluted to an ink with a viscosity suitable for printing. This method of ink preparation is chosen to allow a dispersion of the particles using a triple roll mill. Good dispersion results can be expected using this approach [13]. The triple roll mill process requires an increased amount ofsolid substance to achieve optimum homogenization.

The ideal dispersion is reached as all agglomerates are broken and the particles are completely wetted by the solvent. With the high shear rate and the compressive force, which affect the particles in the roll mill, a very homogenous dispersion is achieved. To break all agglomerates, the gap size in the roll mill is decreased with each process step, resulting in optimum wetting of all the particles [7].

For the conductor line ink silver particles SP11000-25 (Ferro GmbH) are used. The ink for the ferrite core is based on high permeability NiCuZnFeO-particles provided by HITK e.V. [8]. The main properties of the particles are summarized in Table I.

For the formulation of the inks, three solvents are selected. All three solvents are organic, nonpolar, and compatible with the used particles. Table II lists the used solvents.

For the stabilization of the particles, a 1 to 5 weight percentage of cellulose derivatives are used as an additive. To optimize the characteristics of the inks, the application of further dispersing additives is recommended. Due to their surface properties, especially their high specific surface area, the ferrite particles tend to form a slurry with large agglomerates during the dispersing process, especially if the amount of stabilizing additive is too low or the solid substance amount is too high. This effect strongly depends on the used solvent and additives and leads to an unprintable ink. All inks are characterized by analysis of the viscosity and sedimentation behavior.

Fig. 1 shows the viscosity measurement of the ferrite inks at different shear rates. All inks have a solid substance amount (SSA) of 30% weight (wt%) but a varying amount of additive relative to the SSA. The temperature at all measurements is 40°C. Obviously, the additive smoothes and lowers the viscosity curve for lower shear rates. With a shear rate greater than

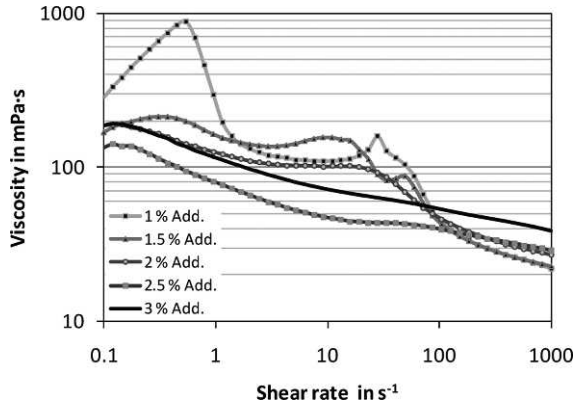

Fig. 1. Shear viscosity of ferrite inks with solvent 1 and different amounts of additive.

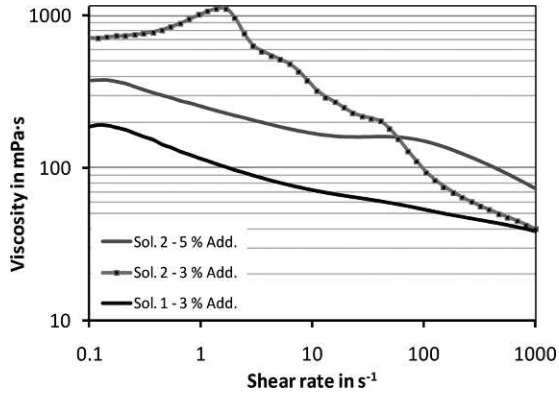

Fig. 2. Shear viscosity of ferrite inks with different solvents and additive amounts.

100 s^{-1}, the viscosity is slightly increased by the additive as expected and shows a linear shear thinning behavior.

The inks with 2.5% of additive and more abruptly no longer show the formation of the agglomerated slurry and show improved sedimentation behavior.

Fig. 2, shows viscosity behavior using a different solvent (solvent 2). The pure viscosity of the solvent as well as its viscosity with the additive is very close to solvent 1. Nevertheless, when ferrite particles are added it shows a different behavior for low shear rates. To achieve an ink without getting the mentioned slurry, 5% of additive is required. Regarding printing viscosity, which is the viscosity at high shear rates, it is found to be too high for the print head. The head requires an ink viscosity in the range of 7 to 50 mPas.

The viscosity depends on the solid substance content, the additive amount, and the temperature. To decrease the viscosity of the inks, a lower additive and a lower solid substance amount are suitable. Also, small amounts of an additional solvent (solvent 3) can decrease viscosity. With some optimization steps, inks are composed that are stably printable. Finally, a ferrite ink containing solvent 1 and 3 (ratio 9:1) is printable with a solid substance amount of 30 wt% and 2 wt% additive relative to this. The silver ink is based on solvent 1 with a solid substance amount of up to 50 wt% and 2 wt% additive.

Downloaded from http://meridian.allenpress.com/jmep/article-pdf/7/4/205/2258973/imaps_258.pdf by guest on 01 November 2022

Printing Equipment

Once an ink formulation is found that meets the requirements of the printing system, the parameter adaption has to be determined. First the ink is tested on a self-engineered printing system consisting of a planar motor (HIWIN LMSP-X2) and a single nozzle piezo print head (Microdrop; 50, 70 or 100 μm nozzle). The system is equipped with a nozzle surveillance camera and stroboscopic LED to investigate the stability of the drop formation. The ink meets the requirements when it shows a long-term stable drop formation and when it does not leave an excessive residue of particles after first flushing and cleaning the head.

Additionally, the printing system is equipped with a heating plate to heat the substrate for quick solvent evaporation. This allows observation of the behavior of the ink on the substrate and is an opportunity to learn about wetting and drying behavior at different temperatures.

Second, the proved ink is tested on the appropriate printing system. In this case it is a modified Xenjet 4000 printer with a Xaar HSS 1001 print head. Its side-shooter design and through-flow system, which moves the ink vertically and directly above the nozzle plate, provides exceptional operational latitude for a wide range of fluids and suspensions. The recirculation removes air bubbles and clogging agglomerates and leads to self-recovery of failing nozzles. The operational range of the head is specified to a viscosity of 7 to 50 mPas. The nozzle gap is 141 μm per row and the two rows are displaced by half a gap (70.5 μm). That leads to the preset resolution of 360 dpi. As the resolution is fixed, it is important to control the drop volume to reach the desired structures on the substrate [14]. This can be achieved in two ways. First, the HSS 1001 allows for adopting the volume with seven linear scaled drop sizes from about 6 pL to 42 pL. Second the drop size depends on piezo actuating voltage settings.

To ensure reproducible drop formation and to adjust ink viscosity, the printing system is additionally equipped with a heating system that keeps the ink at a moderate temperature in the reservoir and heats it up in a double-pipe heat exchanger on its way to the print head. Maximum printing temperature is up to 50°C. The layout of the recirculation system is kept simple and optimized to avoid dead spaces where ink can begin to sediment. The system is driven by a peristaltic pump that does not contact the ink and that guarantees a constant through flow. Thus continuous operation over of several days is possible.

Substrate Coating

Inkjet printing is flexible and cost-efficient in production because it is a maskless deposition method. However, without a mask placing the material reliably to the location where it is needed, and to keep it there, is more complex.

Common substrates used in ceramic interconnects are conventional alumina substrates (96% alumina). These substrates generally show a disadvantageous wetting behavior for inkjet printing due to their high surface energy and their low contact angle (<5 °) with nonpolar solvents [3]. A general consideration of the relevant aspects is helpful. Assuming the shape of the flying drop is a sphere with the initial radius R_0 and the volume

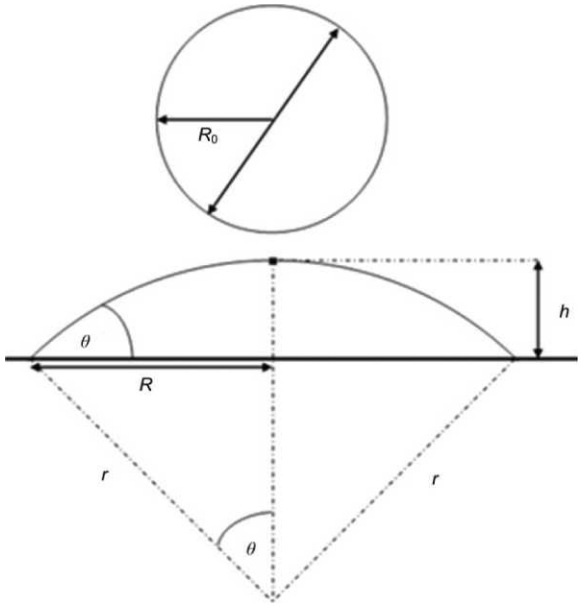

Fig. 3. Geometrical data of the flying and sessile drop with spherical cap laying on substrate.

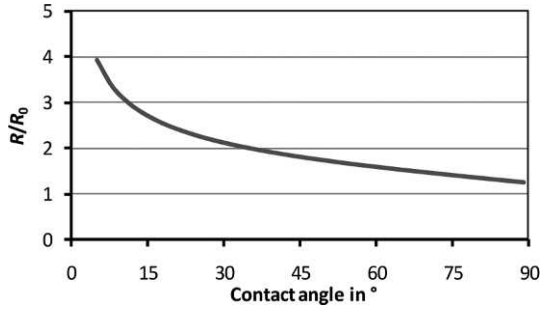

Fig. 4. Ratio of spot and drop radii depending on contact angle.

$$V_0 = \frac{4}{3}\pi \cdot R_0^3 \tag{1}$$

and further, that the shape of the resulting spot is a spherical cap with height h and radius r, the resulting spot radius, R, is mainly influenced by the individual contact angle, θ, between the ink and substrate. The volume of the cap can be calculated by

$$V_{\text{spot}} = \frac{\pi}{3} \cdot \left(\frac{R}{\sin\theta}\right)^3 \cdot (1-\cos\theta)^2 \cdot (2+\cos\theta). \tag{2}$$

Fig. 3 shows the geometrical data of the flying drop and the deposited ink on the substrate. Assuming a constant drop volume, the resulting ratio of radii

$$\beta(\theta) = \frac{R_0}{R} = \frac{1}{\sin\theta} \cdot \sqrt[3]{\frac{(1-\cos\theta)^2 \cdot (2+\cos\theta)}{4}} \tag{3}$$

can be described as a function of the contact angle θ. Fig. 4 shows this relation.

Downloaded from http://meridian.allenpress.com/jmep/article-pdf/7/4/205/2258973/imaps_258.pdf by guest on 01 November 2022

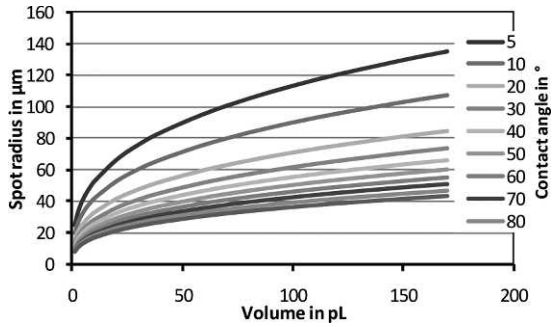

Fig. 5. Spot radius depending on drop volume and contact angle.

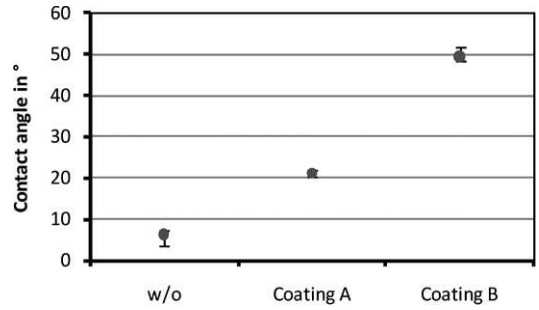

Fig. 6. Change of contact angle applying a substrate coating.

In the case of inkjet printing, it is more convenient to modify this relation by showing the resulting radius

$$R = (\sin\theta) \cdot \sqrt[3]{\frac{3 \cdot V_0}{(1-\cos\theta)^2 \cdot (2+\cos\theta) \cdot \pi}} \qquad (4)$$

as a function of the adjustable factors V_0 and θ. This can be illustrated by an array of curves for different contact angles (Fig. 5).

For fine-line inkjet printing, two approaches are possible for increasing the contact angle. One is to change the solvents, which would affect the previous steps of paste and ink preparation. A second approach would be the modification of the substrate by surface treatment. Very effective and inexpensive is substrate coating, which is already applied in the inkjet paper industry [15]. The choice of suitable coating material is limited by the desired properties. These are, beside a relevant increase of the contact angle, a reduction of ink blurring, compatibility to the used solvents, good adhesion between particles and substrate after drying, compatibility to sintering process and subsequently no changes in the electrical properties. For industrial application an easy coating technique is fundamental.

In this part of the experiment two substrate coatings are tested. Coating A is a solution of a cellulose derivate in a polar solvent at an amount of 5 wt%. This coating can be applied with either spin coating or inkjet printing. Coating B is a conventional coating dispersion of 30 wt% alumina particles with polyvinyl acetate (PVA) in water. It can be applied with spin coating technique. The thickness of both coatings has a negligibly small influence on the resulting contact angle.

Fig. 6 shows the contact angle of a particle ink on an alumina substrate with and without coating. For a 100 pL drop, the resulting spot size is reduced from 120 to 70 µm on coating A and to 50 µm on coating B.

As the results show, increasing the contact angle is an effective way to reduce feature size especially when using an ink-substrate combination with a naturally low contact angle. The effect gets smaller for initially higher contact angles. The decrease of the drop volume is the last option to further decrease the spot radius. An increase of the contact angle leads additionally to an increased load of solid substance that is applied per area. The reduction of drop volume is attended by a increased reduction of applied solid substance load. This induces an increasing number of required printing swathes to reach the same thick-film structure heights. For example, assuming a contact angle of 50°, a reduction of drop volume from 100 to 50 pL reduces the line width from 50 to 40 µm. However, the number of required swathes, and thus the valuable printing time, is increased by a factor of 1.6 to reach an equivalent height.

Two disadvantages of coating B are revealed during the experiments. First, the contact angle is too high for the used print head because sufficient contact of neighboring spots is not reached, even at the highest volume that can be jetted. Second, after firing, the structures do not adhere well to the coating and peel off in the case of silver lines. The necessary sintering temperature peak of 900°C is too low for the alumina particles. An adoption of particle size and therefore reduction of the required sintering temperature could be an applicable solution. The electrical properties might also be affected by the alumina particles, which could not be investigated this time due to the process incompatibility.

Most print heads allow for control of the drop formation and thus the resulting drop volume and velocity [14, 16]. The drop volume is especially closely related to the resulting grid pattern (resolution), and is specified by terms of volume/area or mass/area (e.g., µg/mm^2). The optimum of this parameter can be identified for a certain system of ink and substrate depending on contact angle.

Regarding a line, five characteristic patterns can be pointed out. If the spot diameter is smaller than the drop spacing (Δx), individual spots remain and do not form a continuous line. Further reduction of spacing or, in the case of the HSS 1001 print head, a larger drop volume (due to fixed nozzle pitch) leads to a scalloped line narrower than the single spots. In case the ideal distance between the spots is reached, a homogeneous line with narrowest diameter is formed. This important transition is shown in Fig. 7 (*top*). In the middle, the line is still scalloped. On the left side (lower contact angle, smaller volume) the line is almost completely closed, and on the right side, the optimum spot diameter is reached. At low contact angles the optimum ratio $R/\Delta x$ is generally approximately 0.65.

If the spacing between the spots is further reduced (or the drop volume is further enlarged), bulging occurs. The final pattern is called stacked coins. It occurs only when the substrate is heated so high that the evaporation time is shorter than the jetting frequency. This model can be expanded to block shaped structures consisting of more than one line. Fig. 8 shows two block-shaped elements with different stages of area morphology.

Due to the drop placement deviation on the left side, several morphologies can be found, from single spot to partially homogeneous surface. On the right side, the distance between

Downloaded from http://meridian.allenpress.com/jmep/article-pdf/7/4/205/2258973/imaps_258.pdf by guest on 01 November 2022

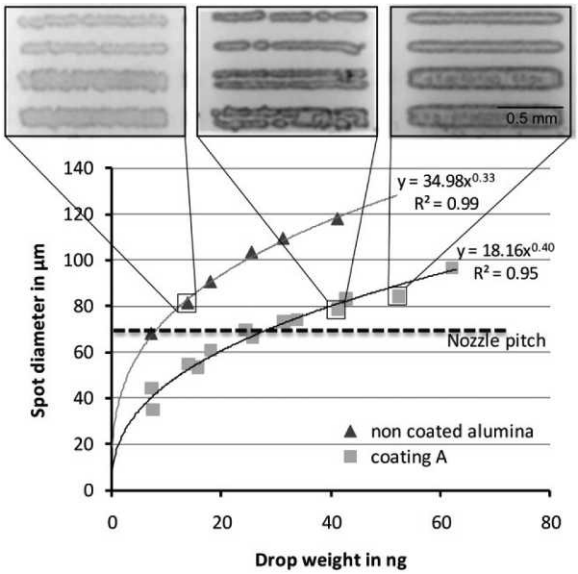

Fig. 7. Influence of substrate coating and drop volume on spot radius *R* and line morphology.

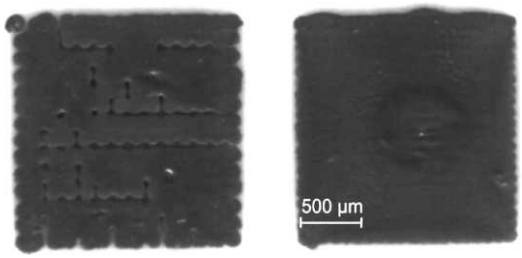

Fig. 8. Block shaped element below and above optimum ink volume per area.

the drops is lowered by factor of $\sqrt{2}$ and therefore complete junction is achieved, although the positioning accuracy does not rise. However, the different drying speed from the edges to the middle leads to bulging and inhomogeneous surface in the middle. Considering that the ink amount is doubled between these elements, enough dosing stages in between exist. There are three possible approaches to reach a more homogeneous result. The drop distance could be increased, the drop volume could be decreased, or the drying speed could be increased.

Finally, changes in the actual surface during printing have to be taken into account. Usually more than one printing swathe is required to reach the desired structure height. The interaction with the initial substrate is important for the ink that is placed with the first swathe, as shown previously. Either modification or coating of the surface is an approach to simplify the deposition of the first layers. However, after the first, and also after all following printing swathes, the surface (for the actual placement of drops) changes significantly. The appearance of the following layers is increasingly influenced by the number of previously printed layers, namely, by their drying states and of course by the now appearing contact angle.

To investigate the behavior of an ink on a changing subsurface, alumina substrates are coated with one to five layers of silver ink and coating A. After complete drying, variable ink

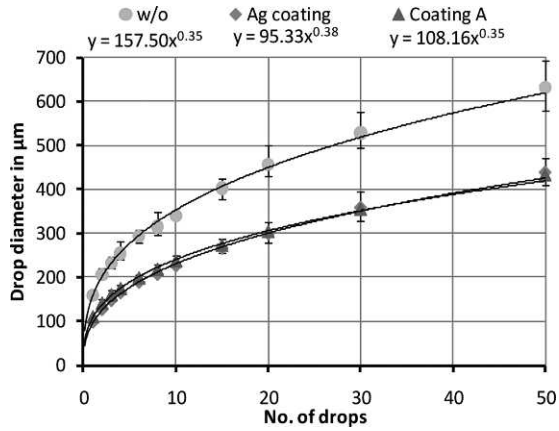

Fig. 9. Spot radius for different drop volume and subsurfaces.

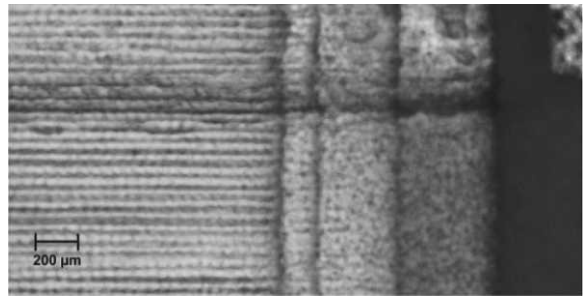

Fig. 10. Appearance of a waved surface structure parallel to printing direction at the forth layer of silver.

volumes of the silver ink are deposited on the coatings. For both kinds of coating, the difference in resulting drop diameter is almost independent from the number of coating layers (1-5 layers). Therefore, the individual results of the coatings are summarized. Fig. 9 shows the different behaviors of the silver ink on an uncoated substrate and on the two different coatings.

By coincidence, the resulting drop diameters on coating A and on silver are similar. This means that this ink behaves similarly at the first and the second printing swathe on any substrate with coating A. This is optimal for production process, as no local variations in drop volume need to be considered to guarantee homogeneous line width. Furthermore, the homogeneity of height is improved.

In case of an inductor with a ferrite core, it is fundamental that the silver and the ferrite inks are printed on the substrate as well as on each other. The line formation of the silver ink on a ferrite bottom layer tends to light bulging and blurring as the contact angle on ferrite is smaller than on coating A and silver.

As mentioned earlier, another parameter that influences ink behavior is the homogeneity of the subsurface. One main reason for inhomogeneities are the different placement conditions of drops placed parallel and vertical to the printing direction. It is likely that a waved profile is built up parallel to the printing direction. Fig. 10 shows this effect appearing with the fourth silver layer. The effect should be avoided by adaption of formation factors, e.g., the drying speed, to guarantee a homogeneous structure height and similar subsurfaces for the following layers of ink.

Downloaded from http://meridian.allenpress.com/jmep/article-pdf/7/4/205/2258973/imaps_258.pdf by guest on 01 November 2022

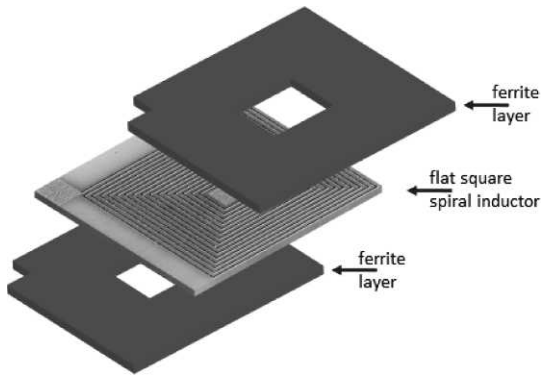

Fig. 11. Scheme of a multilayer inductor with ferrite core.

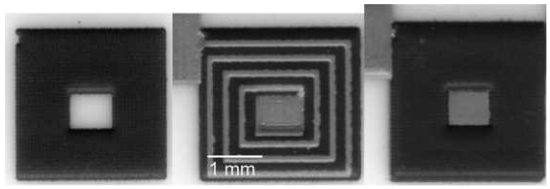

Fig. 12. Stages of a real inkjet printed inductor with a ferrite core.

Construction and Calculation

The basis for a thick-film inductor design is a conductor forming a series of meanders or a flat spiral, either square or circular. When using a multinozzle inkjet print-head, it is much more accurate to apply the square design. Due to the pixel-based layout data, the square design leads to an equidistant gap between the drops. It is preset by the print-head resolution. The circular design leads to a relative gap size changing from 1 to $\sqrt{2}$ and therefore, as shown above, to a more inhomogeneous line formation. It is more susceptible to inaccuracies of drop placement, which lead to shorts in the conductor.

For multilayer design with ferrite (Fig. 11), in a first step the bottom layer of the ferrite core must be printed. This is done swathe by swathe with intermediate drying of a few seconds to avoid a strong fluid and particle flow. The first firing step common for thick-film inductors is abandoned to save the firing time. Subsequently, the required number of conductive layers is printed directly on the dried ferrite bottom. After drying, the cover layer of the ferrite core is printed. Finally, all layers are cofired. In Fig. 12 the stages of building up an inductor by inkjet printing are shown.

The design of the inductors is not chosen or optimized for any electrical application, but should give an idea of the capabilities of inkjet printing.

For a first step inductors without ferrite core are printed. In addition to the flat square spiral, the meander layout is investigated as a possible alternative. Additionally, the number of printing swathes, later also called layers, is varied to investigate their effect on geometrical and electrical properties. Last, the ratio ε of line pixels and space pixels between the conductor lines is reduced from 3 to 2. The size of the inductors is also varied in three steps. Typical dimensions are listed in Table III.

Table III
Geometrical Dimensions of Inductors ($\varepsilon = 3$)

Design	Area	Turns/ Segments	Conductor Length
Unit	mm^2	1	m
Spiral small	6.4	3.25	0.19
Spiral medium	25.8	7.25	0.87
Spiral large	103	15.5	3.65
Meander small	6.4	4	0.25
Meander medium	25.1	7	0.79
Meander large	105	16	3.54

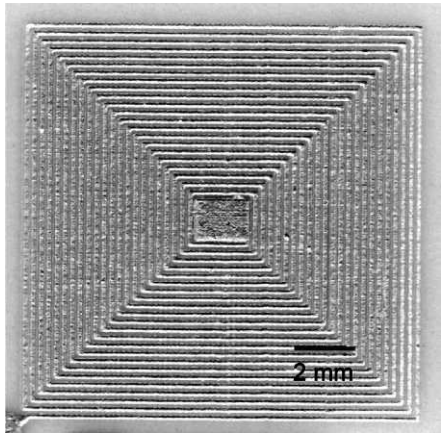

Fig. 13. Flat coil inductor with a line to space ratio of 3:1 (ε=3).

The theoretical calculation of the inductance of wire loops is not the aim of this paper; this has already been discussed in detail [17]. For air-core flat rectangular spiral thick-film inductors, a variety of approximation techniques exist [18] that are not further discussed here.

Geometrical and Electrical Results

The geometrical properties of the printed structures are measured after drying and firing using a light microscope with a measurement unit and a white light interferometer. The electrical properties are analyzed at 1 MHz with a high precision LCR meter. The uniformity of the lines of a large square coil inductor is shown in Fig. 13. With the preset of $\varepsilon = 3$, the theoretical line distance is 282 μm. The printed structure is built up by 20 printing swathes. It has a mean line to space ratio of approximately 95 μm to 185 μm. The thickness after drying is approximately 10 μm, and after firing it is reduced to approximately 8 μm.

The meander design shows similar geometrical results and is as reliably printable as the square spiral design. Due to the printer properties, the line formation in printing direction is of higher quality and shows a better straightness of the edges.

Fig. 14 illustrates a large meander inductor after firing with a ratio $\varepsilon = 2$. The medium line distance is 211 μm, and the structure is built up by 10 printing swathes. It has a mean line to space ratio of approximately 95 μm to 115 μm. The thickness after drying is approximately 6 μm, and after firing it is reduced to approximately 5 μm.

Downloaded from http://meridian.allenpress.com/jmep/article-pdf/7/4/205/2258973/imaps_258.pdf by guest on 01 November 2022

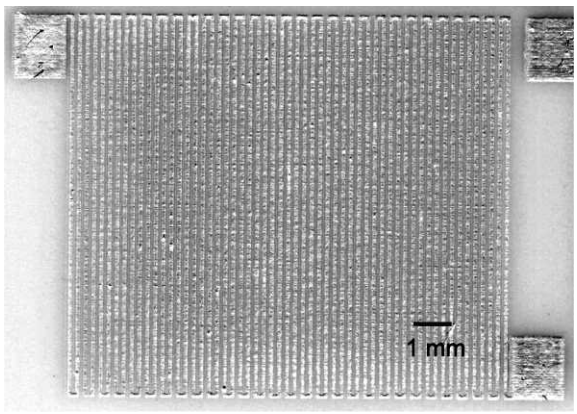

Fig. 14. Flat meander inductor with a line to space ratio of 2:1 ($\varepsilon = 2$).

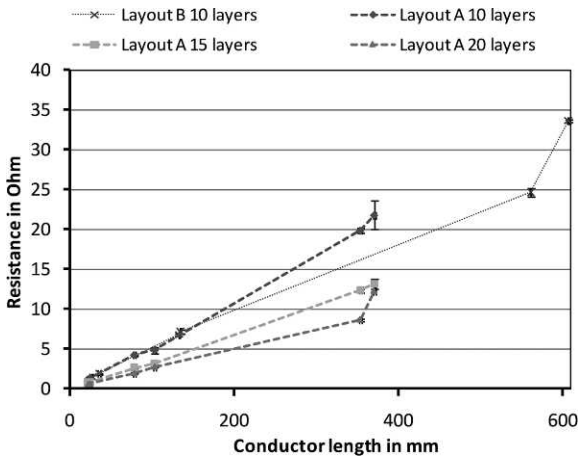

Fig. 15. Resistance of layout A ($\varepsilon = 3$) and B ($\varepsilon = 2$) in relation to the conductor length.

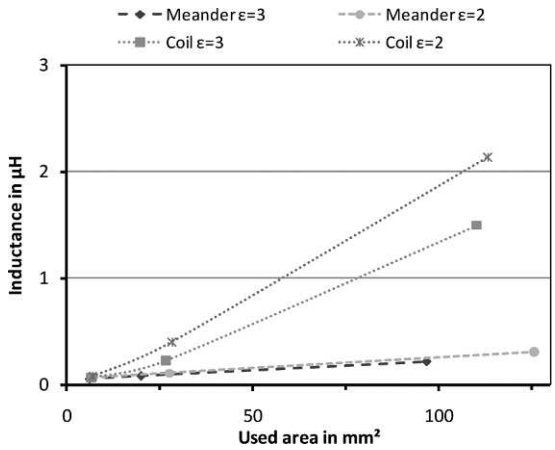

Fig. 16. Inductance of meander and coil layout for $\varepsilon = 3$ and $\varepsilon = 2$.

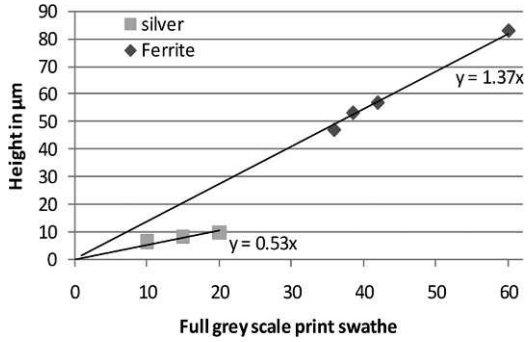

Fig. 17. Layer thickness of the printed silver lines and ferrite cores.

An important characteristic for the silver structure is its resistance. Considering the sheet resistance, as usual for thick-film structures, the value decreases proportionally to the number of applied layers of ink. For 10 layers, a value of 4.8 mΩ/square is achieved; for 15 layers, 3.6 mΩ/square; and for 20 layers, 2.4 mΩ/square. Fig. 15 shows the resistance and the appropriate variance of all printed structures. For the small structures, the three-sigma range is lower than 10%. The larger the structures, the more sensitive their values are to inhomogeneities in drop formation and contamination. It has to be mentioned that the samples are not printed under clean room conditions. The inductance of all printed structures is presented in Fig. 16. The illustration of the values has changed when compared with Fig. 15. Although the resistance is almost independent from the general inductor design and the line to space ratio, the inductance strongly depends on these parameters. However, it is independent of the thickness of the inductor at the evaluated frequency point. The corresponding standard deviations are again considerably low. For example, the inductance of all large coils with $\varepsilon = 3$ has a standard deviation of less than 2%.

The meander design shows poor inductance values. Compared with spiral design they are reduced by a factor of five at a similar area. However, the standard deviation is low as well. The quality factor at 1 MHz is in the range of 0.7 to 1.8 and strongly depends on the number of silver layers.

The printed inductors with ferrite core are characterized geometrically, considering their height and the homogeneity of their surface. The ferrite particles are sensitive to inhomogeneous drying. Cracking occurs easily if ink flow takes place, which might be initiated by improper drying. Furthermore, cracking is likely to appear directly above the silver lines. This is due to stress caused by structure shrinkage during the sintering process. First layers of the upper ferrite layer have to level the space between the conductor lines. If this is not done, or the ink is not placed accurately, cracks occur.

Fig. 17 shows the layer thickness of the silver lines and ferrite cores, depending on the number of printing swathes. The expected linear increase can be seen, but the difference in slope is remarkable, as the product of volume fraction and drop volume does not differ much. A high porosity of the printed ferrite layers is assumed. However it is not proven, as the sintering shrinkage is similar at approximately 15% for ferrite and 20% for the silver after 2 hours at 900°C. A further analysis of microstructure should be performed.

The shape of the completely inkjet printed inductors with ferrite core at different size is illustrated in Fig. 18. The size of

Downloaded from http://meridian.allenpress.com/jmep/article-pdf/7/4/205/2258973/imaps_258.pdf by guest on 01 November 2022

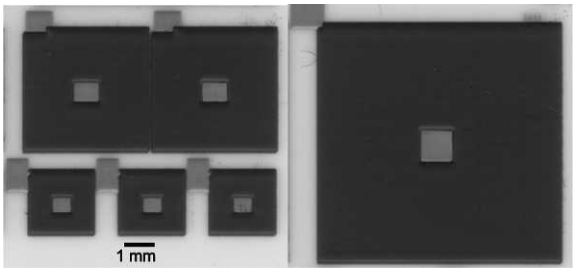

Fig. 18. Inkjet printed inductors with ferrite core in different sizes.

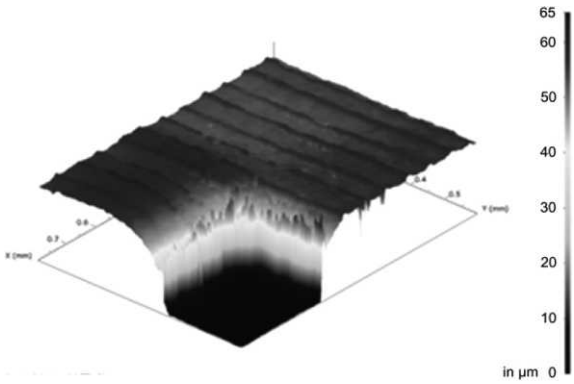

Fig. 19. Surface scan of a ferrite sector (0.6×0.8 mm^2) measured with a white light interferometer.

the inductors can be scaled in pixel steps of 70.5 µm, depending on the coil layout and the required number of turns. It is only limited by the substrate size. The structures show an excellent sharpness of the edges.

In Fig. 19 a surface scan of a ferrite section measured with a white light interferometer reveals a slightly waved surface in printing direction with small strias at the interfaces, as mentioned before. The absolute height (dried) of the structure is 60 µm, the height of the rills is less than 2 µm. As no further ink is printed on top, this effect is acceptable.

The enhanced electrical properties of these inductors with ferrite core should be provable after sintering at 900°C. However, the measured inductance increase is negligible. Dilatometric results show a maximum shrinkage rate at 840°C with no complete densification even at 950°C. Higher temperatures would lead to problems with the silver conductor. Additionally, due to different coefficients of thermal expansion α, the used alumina substrate ($\alpha \approx 7.5 \cdot 10^{-6}$ K^{-1}) and the ferrite ($\alpha \approx 9.9 \cdot 10^{-6}$ K^{-1}) are not thermally compatible. This leads to thermal stress and to peeling-off or cracking within the ferrite structure. For efficient use of the electrical respectively magnetically properties of the ferrite material, it should be further adapted or other substrate and conductor line materials have to be taken into account.

Conclusion

A promising ink composition with a high permittivity ferrite material is realized with 30 wt% solid substance content. Using inkjet technology, ferrite cores are printed to embed fine-line silver inductor coils. It is shown that the controlled deposition of the ink on the substrate is the key element to control the geometrical and also the electrical properties. For print heads with a fixed resolution, the contact angle and the drop volume are the main factors influencing the structures morphology. The contact angle can be adapted by substrate coating, without changing the sintering behavior or the electrical properties. The drop volume can be adjusted easily to reach the desired surface morphology. With this basic knowledge an approved silver ink is applied. Meander and square coils are reliably generated down to about 100 µm/100 µm pitch on alumina substrate with very low variance in electrical values. The principle realization of thick-film inductors with ferrite core by inkjet printing is shown.

It is demonstrated that inkjet technology has the capability to build up all types of passive electronic components reliably.

References

[1] A. Albertsen, K. Aruga, K. Kobayashi and K. Koiwai, "Combined manufacture method for high density LTCC-substrates: thick film screen-printing, ink-jet, post-firing thin-film processes and laser-drilled fine-vias." *Proceedings of the 4th International Conference on Ceramic Interconnect and Ceramic Microsystems Technologies*, Munich, Germany, April, 2008. Washington, DC: International Microelectronic And Packaging Society.

[2] D. Cibis and K. Krueger, "DoD-printing of conductive silver tracks." *Proceedings of the 1st International Conference on Ceramic Interconnect and Ceramic Microsystems Technologies*, Baltimore, Maryland, April, 2005. Washington, DC: International Microelectronic And Packaging Society.

[3] U. Currle, "Funktionelle Partikeltinten für den Inkjet-Druck von mikroelektronischen Strukturen" (*Functional particle inks for inkjet printing of microelectronic structures*). Dr.-Ing. thesis, Helmut-Schmidt-University, Hamburg, 2010.

[4] St. Barth, M. Arnold, D. Grützmann, B. Pawlowski, P. Rothe and Th. Bartnitzek, "Low sintering high-k materials for LTCC application." *Proceedings of the 4th International Conference on Ceramic Interconnect and Ceramic Microsystems Technologies*, Munich, Germany, April, 2008. Washington, DC: International Microelectronic And Packaging Society.

[5] H. Naghib-Zadeh. C. Glitzky, and T. Rabe, "$BaTiO_3$-based high-k composition with LTCC compatible sintering temperature." *Proceedings of the 4th International Conference on Ceramic Interconnect and Ceramic Microsystems Technologies*, Munich, Germany, April, 2008. Washington, DC: International Microelectronic And Packaging Society.

[6] St. Barth, "Entwicklung niedrigsinternder Funktionswerkstoffe für LTCC-Bauelemente" (*Development of low-sintering materials for LTCC elements)*. Deutsche IMAPS-Konferenz, Munich, Germany, October, 2008. Washington, DC: International Microelectronic And Packaging Society.

[7] M. Wassmer, W. Diel, and K. Krueger, "Inkjet printing of post-fired thick-film capacitors." *Proceedings of the 5th International Conference on Ceramic Interconnect and Ceramic Microsystems Technologies*, Denver, Colorado, April, 2009. Washington, DC: International Microelectronic And Packaging Society.

[8] J. Muerbe and J. Toepfer, "Ni-Cu-Zn Ferrites for low temperature firing: I. Ferrite composition and its effect on sintering behavior and permeability," Journal of Electroceramics, Vol. 15, pp. 215-221, 2005.

[9] H.-J. Kim, Y.-J. Kim, and J. Kim, "An integrated LTCC inductor embedding NiZn ferrite." IEEE Transactions on Magnetics, Vol. 42, No. 10, pp. 2840-2824, October, 2006.

[10] R. Hahn, St. Krumbholz, H. Reichl, "Low profile power inductors based on ferromagnetic LTCC technology." *Proceedings of the 56th Electronic Component and Technology Conference*, San Diego, California, May, 2006. Piscataway, NJ: Institute of Electrical and Electronics Engineers, pp. 528-533.

[11] W. Diel, M. Waßmer, K. Krüger, H. Naghib-Zadeh and T. Rabe: "Einfluss unterschiedlicher Dielektrika bei der Realisierung von

Downloaded from http://meridian.allenpress.com/jmep/article-pdf/7/4/205/2258973/imaps_258.pdf by guest on 01 November 2022

Dickschichtkondensatoren im Tintenstrahldruck" (*Influence of different dielectica on the realization of thick-film capacitors by inkjet printing)*. Deutsche IMAPS-Konferenz, Munich, Germany, October, 2009. IMAPS Deutschland e.V., Ganghofen.

[12] U. Currle, M. Wassmer, K. Krueger, "Particle Inks for Inkjet Printing of Electronic Components." *Proceedings of Digital Fabrication 08,* pp.702-706 Pittsburgh, Pennsylvania, September 2008. Springfield, VA: Society for Imaging Science and Technology.

[13] Lin-Hung-Wen, Hwu-Wen-Hwa, and Ger-Ming-Der: "The dispersion of silver nanoparticles with physical dispersal procedures," Journal of Materials Processing Technology, Vol. 206, pp. 56-61, 2008.

[14] D. Soltman and V. Subramanian, "Inkjet-printed line morphologies and temperature control of the coffee ring effect," Langmuir, Vol. 24, No. Issue 5, pp. 2224-2231, (2008).

[15] D. Cibis and K. Krueger, "Influencing Parameters in Droplet Formation for DoD Printing of Conductive Silver Tracks." *Proceedings of the 4th International Conference on Ceramic Interconnect and Ceramic Microsystems Technologies*, Munich, Germany, April, 2008. Washington, DC: International Microelectronic And Packaging Society.

[16] A. Storeck and Ch. Batz-Sohn, "Novel inkjet coating alumina." *Proceedings of the 22nd International Conference on Digital Printing Technologies*, Denver, Colorado, September, 2006. Springfield, VA: Society for Imaging Science and Technology.

[17] M. Thompson, "Inductance calculation techniques, Part I/II:Approximations and handbook methods." Power Control and Intelligent Motion, December, 1999. Available from: http://www.pcim.com.

[18] H. Greenhouse, "Design of planar rectangular microelectronic inductors." IEEE Transaction on Parts, Hybrids, and Packaging, Volume PHP-10, No. 2, pp. 101-109, June, 1974.

Downloaded from http://meridian.allenpress.com/jmep/article-pdf/7/4/205/2258973/imaps_258.pdf by guest on 01 November 2022